

Supporting Information

Heterostructures of MXene and N-doped graphene as highly active bifunctional electrocatalysts

Si Zhou, Xiaowei Yang, Wei Pei, Nanshu Liu, Jijun Zhao*

*Key Laboratory of Materials Modification by Laser, Ion and Electron Beams (Dalian University
of Technology), Ministry of Education, Dalian 116024, China*

* Corresponding author. Email: zhaojj@dlut.edu.cn

To model the heterostructures of N-doped graphene on MXene monolayers, we used a supercell consisting of 5×5 graphene unit cells and 4×4 unit cells for Ti_2C , V_2C , Nb_2C , and $\sqrt{19} \times \sqrt{19}$ unit cells for Mo_2C MXene monolayer, respectively. The Ti_2C monolayer was stretched and the other MXenes were compressed to fit the graphene supercell. For each graphene/MXene heterostructure, we considered four different models, with the N atoms in either the graphitic or pyridinic form, and the surface C (N) atoms in different positions relative to the topmost metal atoms in MXenes (Fig. S1-4). The four models exhibit similar structural and electronic properties as demonstrated by Table S1 and Fig. S11-13.

To characterize the catalytic activity for oxygen reduction reaction (ORR), we considered the four electron pathway for ORR in alkaline media:¹



The Gibbs free energy of formation for the i^{th} step can be calculated by

$$\Delta G_i = \Delta E_{\text{DFT}} + \Delta \text{ZPE} - T\Delta S - eU \quad (\text{S5})$$

where ΔE_{DFT} , ΔZPE and $T\Delta S$ are the changes of DFT total energy, zero-point energy and entropy during the reactions, respectively; T is temperature; U is the electrode potential; e is the electron charge transfer. ΔZPE and ΔS can be obtained by the NIST-JANAF thermodynamics table for gaseous molecules² and by calculating the vibrational frequencies for the reaction intermediates, respectively (Table S7).

Within the framework of standard hydrogen electrode (SHE) model,³ the difference of Gibbs free energies between OH⁻ anions and electrons can be related to those of H₂O and H₂ molecules via the following relation:

$$G(\text{OH}^-) - G(e^-) = G(\text{H}_2\text{O}) - 1/2G(\text{H}_2) + k_{\text{B}}T \cdot \ln 10 \cdot \text{pH} \quad (\text{S6})$$

where the last term is the correction to the Gibbs free energy of OH⁻ anions at a pH value other than zero; k_{B} is the Boltzmann constant. In this work, we consider pH = 14 and $T = 298$ K. Actually, the computed ORR overpotentials are independent on the choice of pH value.⁴ The ORR overpotential is then given by

$$\eta^{\text{ORR}} = \Delta G^{\text{ORR}}/e + U_0 \quad (\text{S7})$$

where $\Delta G^{\text{ORR}} = \max[\Delta G_1, \Delta G_2, \Delta G_3, \Delta G_4]$, and $U_0 = 0.40$ V is the equilibrium potential for pH = 14 and temperature $T = 298$ K.⁵

The HER performance was evaluated by the reaction free energy (ΔG_{H^*}) of hydrogen adsorption:⁶

$$\Delta G_{\text{H}^*} = \Delta E_{\text{H}^*} + \Delta \text{ZPE} - T\Delta S \quad (\text{S8})$$

where ΔE_{H^*} , ΔZPE and ΔS are the differences of DFT total energy, zero-point energy, and entropy between the adsorb H* phase and H₂ gas phase, respectively. The values of ($\Delta \text{ZPE} - T\Delta S$) for our graphene/MXene heterostructures were calculated to be 0.37 eV at $T = 298$ K (Table S7).

Based on Equation S1-8, η^{ORR} and ΔG_{H^*} can be obtained by computing the binding energies of relevant reaction intermediates on various sites of the catalyst surface. Here we refer the binding energies of all the reaction intermediates to the energies of H₂ and H₂O molecules as follows:

$$\Delta E_{\text{OH}^*} = E(\text{OH}^*) - E(^*) - [E(\text{H}_2\text{O}) - 1/2E(\text{H}_2)] \quad (\text{S9})$$

$$\Delta E_{\text{OOH}^*} = E(\text{OOH}^*) - E(^*) - [2E(\text{H}_2\text{O}) - 3/2E(\text{H}_2)] \quad (\text{S10})$$

$$\Delta E_{\text{O}^*} = E(\text{O}^*) - E(^*) - [E(\text{H}_2\text{O}) - E(\text{H}_2)] \quad (\text{S11})$$

$$\Delta E_{\text{H}^*} = E(\text{H}^*) - E(^*) - 1/2E(\text{H}_2) \quad (\text{S12})$$

where $E(^*)$, $E(\text{OH}^*)$, $E(\text{OOH}^*)$, $E(\text{O}^*)$ and $E(\text{H}^*)$ are the DFT total energies of a clean catalyst surface, and that adsorbed by a OH^* , OOH^* , O^* and H^* species, respectively; $E(\text{H}_2\text{O})$ and $E(\text{H}_2)$ are the energies of a H_2O and H_2 molecule in vacuum, respectively. The Gibbs free energy of O_2 is derived from $\text{H}_2\text{O} \rightarrow 1/2\text{O}_2 + \text{H}_2$ using the experimental reaction energy of 2.46 eV to avoid the well-known errors by DFT calculation in describing the high-spin ground state of O_2 molecule.³

The full information for the binding energies of reaction intermediates on the graphene/MXene models is given by Table S3-6. Generally speaking, the four models for each hybrid system exhibit similar surface binding properties and catalytic activities.

The trend of binding capability of the graphene/MXene heterostructures vs. $C p_z$ band center can be roughly understood within the picture of the extended Hückel theory.⁷ The off-diagonal Hamiltonian matrix element $H_{\mu\nu}$, which is correlated to the bonding strength between two atoms μ and ν , can be written as

$$H_{\mu\nu} = K/2(H_{\mu\mu} + H_{\nu\nu})S_{\mu\nu} \quad (13)$$

where $H_{\mu\mu}$ and $H_{\nu\nu}$ are the diagonal elements and in our case correspond to the absolute energy levels of the valence states of the surface C atoms and reaction intermediates, respectively; $S_{\mu\nu}$ is the orbital overlap matrix element and mainly

depends on the distance between atoms μ and ν ; K is the Wolfsberg-Helmholtz constant usually chosen between 1.75 and 2. As the C–O and C–H bond lengths do not vary significantly (within 0.2 Å) in different graphene/MXene models, $H_{\mu\nu}$ is mainly determined by the valence orbital levels of the graphitic sheet. Deeper centers of the C p_z bands lead to lower $H_{\mu\nu}$, and result in stronger binding with the reaction intermediates.

Table S1 Structural and electronic properties of N-doped graphene on MXene monolayers, including lattice mismatch (δ), interlayer distance (d), vertical buckling of the graphitic sheet (Δd), interlayer binding energy per C atom in graphene (ΔE), number of electrons gained by each C atom in graphene (CT), C p_z band center referred to the Fermi level (ε_{pz}), and work function of the heterostructure (Φ). The graphene sheets doped by graphitic and pyridinic N atoms are indicated by “g” and “p”, respectively.

model	N type	δ (Å)	d (Å)	Δd (Å)	CT (e)	ΔE (eV)	ε_{pz} (eV)	Φ (Å)
G/Ti ₂ C	g	2.12%	2.14	0.08	0.11	-0.36	-4.95	4.53
	p	2.12%	2.13	0.13	0.08	-0.42	-4.95	4.56
G/V ₂ C	g	1.84%	2.11	0.06	0.11	-0.27	-5.66	5.18
	p	1.84%	2.08	0.05	0.07	-0.32	-5.80	5.31
G/Nb ₂ C	g	1.15%	2.42	0.26	0.08	-0.19	-4.97	4.55
	p	1.15%	2.40	0.28	0.06	-0.25	-5.01	4.65
G/Mo ₂ C	g	0.23%	2.39	0.26	0.08	-0.17	-5.09	4.66
	p	0.23%	2.39	0.27	0.07	-0.23	-5.12	4.70

Table S2 Binding energies of OH* (ΔE_{OH^*}), OOH* (ΔE_{OOH^*}), O* (ΔE_{O^*}) and H* species (ΔE_{H^*}), ORR overpotentials (η^{ORR}) and reaction free energy of hydrogen adsorption (ΔG_{H^*}) for the G/V₂C (G/Ti₂C) heterostructure with the graphitic sheet under zero or 1.84% tensile strain (2.12% compressive strain).

Model and site	strain	ΔE_{OH^*}	ΔE_{OOH^*} (eV)	ΔE_{O^*}	η^{ORR} (V)	ΔE_{H^*} (eV)	ΔG_{H^*}
G/V ₂ C	0	0.44	3.63	1.71	0.39	-0.26	0.11
(A-1)	1.84%	0.48	3.67	1.73	0.35	-0.20	0.17
G/Ti ₂ C	0	0.70	3.93	2.56	0.64	-0.03	0.34
(A-3)	2.12%	0.60	3.85	2.51	0.56	-0.12	0.25

Table S3 Binding energies of OH* (ΔE_{OH^*}), OOH* (ΔE_{OOH^*}), O* (ΔE_{O^*}) and H* species (ΔE_{H^*}), ORR overpotentials (η^{ORR}), rate-limit step of ORR (RLS), reaction free energy of hydrogen adsorption (ΔG_{H^*}), and number of electrons gained (CT) for various C sites of the four G/Ti₂C models. The specific model and reaction site are indicated by Letters and numbers, respectively, and their atomic structures are displayed in Fig. S1. The values for the most active sites of freestanding N-doped graphene are also listed for comparison. “GN-g” and “GN-p” represent graphene monolayer doped by graphitic and pyridinic N atoms, respectively.

model and site	ΔE_{OH^*}	ΔE_{OOH^*} (eV)	ΔE_{O^*}	η^{ORR} (V)	RLS	ΔE_{H^*} (eV)	ΔG_{H^*} (eV)	CT (<i>e</i>)
A-1	0.78	3.46	0.87	1.50	OH*	0.11	0.48	-0.06
A-2	1.07	4.23	2.78	0.94	OOH*	0.35	0.72	0.06
A-3	0.70	3.93	2.56	0.64	OOH*	-0.03	0.34	-0.03
B-1	0.83	4.05	2.71	0.76	OOH*	0.23	0.60	-0.37
B-2	1.22	4.36	2.82	1.07	OOH*	0.53	0.90	0.11
B-3	1.13	4.33	2.94	1.03	OOH*	0.41	0.78	0.12
C-1	0.58	3.86	1.44	0.73	OH*	-0.09	0.28	-0.09
C-2	1.27	4.40	2.39	1.11	OOH*	0.54	0.91	0.14
C-3	1.16	4.33	2.98	1.03	OOH*	0.46	0.83	0.10
D-1	0.99	4.16	2.37	0.87	OOH*	0.43	0.80	-0.26
D-2	1.19	4.35	3.11	1.06	OOH*	0.48	0.85	0.18
D-3	1.32	4.34	2.93	1.06	OOH*	0.55	0.92	0.25
GN-g	1.34	4.60	2.88	1.24	OOH*	0.42	0.79	-0.31
GN-p	1.45	4.63	3.17	1.27	OOH*	0.12	0.49	-0.12

Table S4 Same as Table S3 for the G/V₂C models, whose atomic structures are displayed in Fig. S2.

Model and site	ΔE_{OH^*}	ΔE_{OOH^*} (eV)	ΔE_{O^*}	η^{ORR} (V)	RLS	ΔE_{H^*} (eV)	ΔG_{H^*} (eV)	CT (e)
A-1	0.44	3.63	1.71	0.39	OH ⁻	-0.26	0.11	-0.20
A-2	0.43	3.80	1.89	0.51	OOH*	-0.22	0.15	0.05
A-3	0.37	3.66	1.89	0.46	OH ⁻	-0.33	0.04	0.16
A-4	0.46	3.65	1.46	0.60	OH*	-0.20	0.17	0.11
B-1	0.24	3.48	1.71	0.59	OH ⁻	-0.41	-0.04	-0.27
B-2	0.46	3.63	2.09	0.36	OH ⁻	-0.21	0.16	0.14
B-3	0.46	3.65	1.96	0.37	OH ⁻	-0.22	0.15	0.11
B-4	0.84	4.04	2.49	0.75	OOH*	0.18	0.55	0.25
C-1	-0.19	3.10	0.25	1.03	OH ⁻	-0.84	-0.47	-0.10
C-2	0.39	3.58	0.16	1.82	OH*	-0.31	0.06	0.08
C-3	0.40	3.57	1.78	0.43	OH ⁻	-0.28	0.09	0.12
C-4	0.46	3.63	1.91	0.37	OH ⁻	-0.23	0.14	0.13
C-5	0.42	3.61	1.83	0.41	OH ⁻	-0.26	0.11	0.11
D-1	0.25	3.66	1.81	0.57	OH ⁻	-0.22	0.15	-0.32
D-2	0.48	3.70	1.56	0.51	OH*	-0.22	0.15	0.11
D-3	0.50	3.70	1.99	0.39	OOH*	-0.20	0.17	0.12

Table S5 Same as Table S3 for the G/Nb₂C models, whose atomic structures are displayed in Fig. S3.

model and site	ΔE_{OH^*}	ΔE_{OOH^*} (eV)	ΔE_{O^*}	η^{ORR} (V)	RLS	ΔE_{H^*} (eV)	ΔG_{H^*} (eV)	CT (e)
A-1	1.13	4.24	1.38	1.33	OH*	0.40	0.77	-0.13
A-2	0.87	4.19	1.75	0.90	OOH*	0.13	0.50	0.06
A-3	0.68	3.87	2.35	0.58	OOH*	-0.03	0.34	-0.06
A-4	0.90	4.05	2.38	0.76	OOH*	0.10	0.47	0.07
B-1	0.60	3.83	2.42	0.54	OOH*	0.04	0.41	-0.31
B-2	0.81	4.03	2.61	0.74	OOH*	0.06	0.43	0.11
B-3	0.92	4.08	2.20	0.79	OOH*	0.26	0.63	0.14
C-1	0.50	3.65	1.15	0.95	OH*	-0.16	0.21	-0.10
C-2	0.93	4.09	2.80	0.80	OOH*	0.23	0.60	0.04
C-3	1.11	4.23	2.13	0.94	OH*	0.33	0.70	0.13
D-1	0.88	4.04	2.41	0.75	OOH*	0.10	0.47	-0.33
D-2	0.67	3.91	2.62	0.62	OOH*	0.05	0.42	0.05
D-3	0.98	4.18	2.41	0.89	OOH*	0.16	0.53	0.08

Table S6 Same as Table S3 for the G/Mo₂C models, whose atomic structures are displayed in Fig. S4.

model and site	ΔE_{OH^*}	ΔE_{OOH^*} (eV)	ΔE_{O^*}	η^{ORR} (V)	RLS	ΔE_{H^*} (eV)	ΔG_{H^*} (eV)	CT (e)
A-1	0.59	3.81	2.40	0.52	OOH*	-0.15	0.22	-0.26
A-2	0.48	3.78	1.60	0.49	OOH*	-0.24	0.13	-0.01
A-3	0.61	3.85	1.90	0.56	OOH*	-0.11	0.26	0.13
A-4	0.73	3.93	2.19	0.64	OOH*	0.01	0.38	0.16
B-1	0.95	4.12	2.62	0.83	OOH*	0.13	0.50	-0.37
B-2	0.55	3.75	2.08	0.46	OOH*	-0.24	0.13	0.03
B-3	0.91	4.08	2.46	0.79	OOH*	0.21	0.58	0.25
C-1	0.55	3.90	1.05	1.09	OH*	-0.12	0.25	-0.07
C-2	0.40	3.66	1.64	0.43	OH ⁻	-0.32	0.05	-0.10
C-3	0.59	3.87	2.67	0.58	OOH*	0.05	0.42	0.02
C-4	0.70	3.88	1.45	0.84	OH*	-0.02	0.35	0.05
D-1	0.46	3.68	1.91	0.39	OOH*	-0.20	0.17	-0.31
D-2	0.73	4.03	2.24	0.74	OOH*	0.07	0.44	0.14
D-3	0.95	4.14	2.37	0.85	OOH*	0.12	0.49	0.27
D-4	0.91	4.05	2.50	0.76	OOH*	0.22	0.59	0.13

Table S7 Zero-point energy (ZPE) and entropic correction (TS) at $T = 298$ K for reaction intermediates involved in ORR and HER. The values of H_2O and H_2 molecules are taken from the NIST-JANAF thermodynamics table.² The vibrational frequencies of OH^* , OOH^* , O^* and H^* species are calculated on several selected C sites of the graphene/MXene models, and they give almost the same ZPE and TS values. Thus, constant values of ($ZPE-TS$) are used for each type of reaction intermediate throughout the calculations.

Species	ZPE (eV)	TS (eV)	$ZPE-TS$ (eV)
H_2O	0.56	0.67	-0.11
H_2	0.27	0.41	-0.14
OH^*	0.39	0.03	0.36
OOH^*	0.46	0.07	0.39
O^*	0.08	-0.01	0.07
H^*	0.30	0	0.30

Table S8 Reaction free energy of hydrogen adsorption (ΔG_{H^*}) at optimal hydrogen coverage, binding energies of OH* (ΔE_{OH^*}), OOH* (ΔE_{OOH^*}) and O* species (ΔE_{O^*}), and ORR overpotentials (η^{ORR}) for the bottom surface of MXene substrate of the graphene/MXene heterostructures in Fig. S1-4, as well as for standalone O-terminated MXene monolayers. For all the considered systems, formation of OOH* species from O₂ molecule is the rate-limit step of ORR.

system	coverage	ΔG_{H^*} (eV)	ΔE_{OH^*}	ΔE_{OOH^*} (eV)	ΔE_{O^*}	η^{ORR} (V)
G/Ti ₂ C	4/16	-0.10	2.93	5.01	3.68	1.72
Ti ₂ C	1/8	-0.04 ⁸	3.18	4.92	4.06	1.63
G/V ₂ C	3/19	-0.07	2.87	4.92	4.34	1.63
V ₂ C	3/8	-0.02 ⁸	2.53	4.93	4.33	1.64
G/Nb ₂ C	1/16	0.36	3.24	5.11	4.91	1.82
Nb ₂ C	1/8	0.02 ⁸	3.38	5.08	4.93	1.79
G/Mo ₂ C	2/16	0.03	2.96	5.07	3.45	1.78
Mo ₂ C	1/8	0.05 ⁹	2.03	4.89	3.51	1.60

Table S9 Binding energies of OH* (ΔE_{OH^*}), OOH* (ΔE_{OOH^*}), O* (ΔE_{O^*}) and H* species (ΔE_{H^*}), ORR overpotentials (η^{ORR}), rate-limit step of ORR (RLS) and reaction free energy of hydrogen adsorption (ΔG_{H^*}) on various C sites of the G/V₂C heterostructure (model A) with the bottom surface of V₂C terminated by F species. Compared to the O-terminated model, the binding energies raise by about 0.2 eV for OH*, OOH* and H* species and by about 0.4 eV for O* species. The F-terminated systems are still active for ORR catalysis, and the rate-limit step becomes the formation of OOH* species from O₂ molecule.

Model and site	ΔE_{OH^*}	ΔE_{OOH^*} (eV)	ΔE_{O^*}	η^{ORR} (V)	RLS	ΔE_{H^*} (eV)	ΔG_{H^*}
A-1	0.60	3.82	2.34	0.53	OOH*	-0.08	0.29
A-2	0.56	3.78	2.31	0.49	OOH*	-0.14	0.23
A-3	0.55	3.74	2.29	0.45	OOH*	-0.16	0.21
A-4	0.64	3.85	1.75	0.56	OOH*	-0.04	0.33

Table S10 Interlayer distance (d) and reaction free energy of hydrogen adsorption (ΔG_{H^*}) on selected C sites of the N-doped graphene on the M_2C or M_3C_2 MXene monolayer ($M = \text{Ti, V, Nb}$ and Mo). The hybrid systems based on M_2C and M_3C_2 MXenes exhibit very similar surface binding properties and thus are expected to have similar catalytic activities for HER and ORR.

M	Model and site	M_2C		M_3C_2	
		d (Å)	ΔG_{H^*} (eV)	d (Å)	ΔG_{H^*} (eV)
Ti	A-3	2.14	0.34	2.14	0.33
V	A-3	2.11	0.04	2.10	0.04
Nb	C-1	2.42	0.21	2.41	0.20
Mo	B-2	2.39	0.13	2.38	0.12

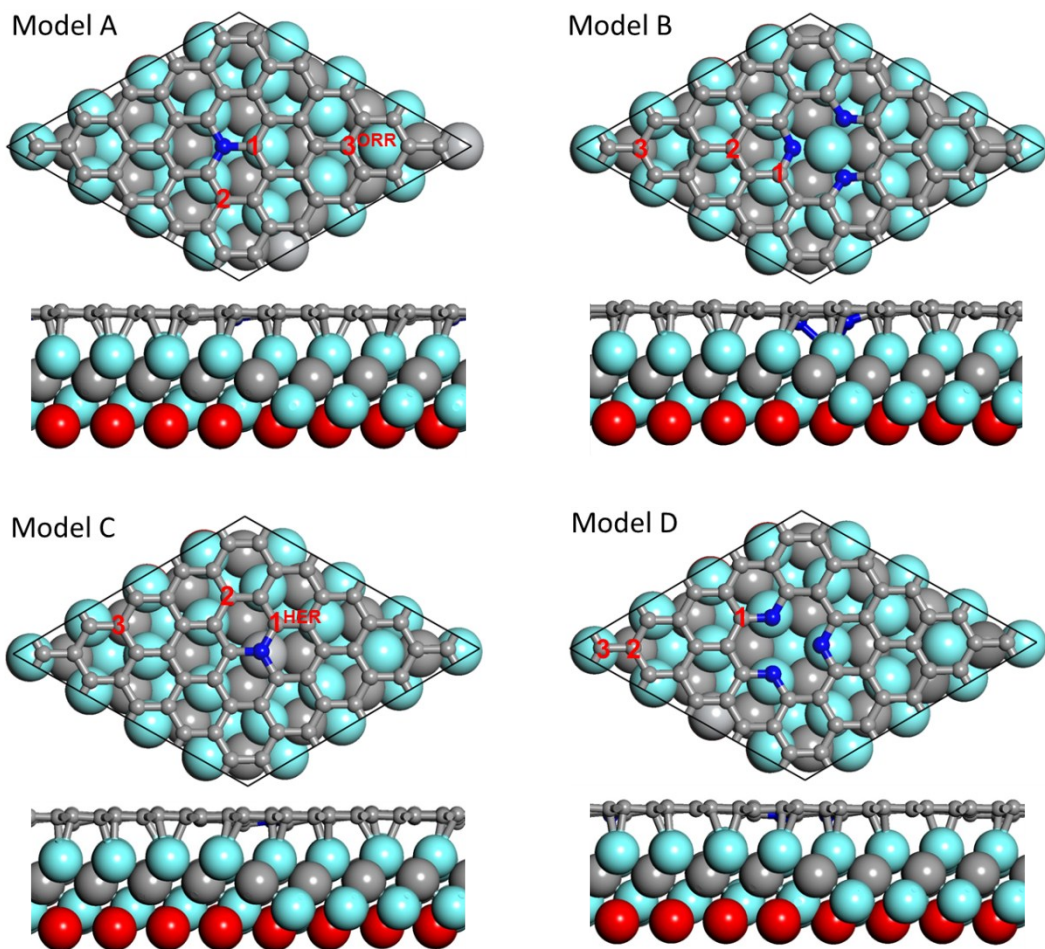


Fig. S1 Four models of N-doped graphene on Ti_2C MXene monolayer. The black boxes indicate the dimensions of the supercells. The red numbers label the C sites, whose binding energies of reaction intermediates and activities for ORR and HER are evaluated and listed in Table S3. The subscripts “ORR” and “HER” indicate the C sites with lowest η^{ORR} and $|\Delta G_{\text{H}^*}|$, respectively. The C, N, O and Ti atoms are shown in grey, blue, red and cyan colors, respectively.

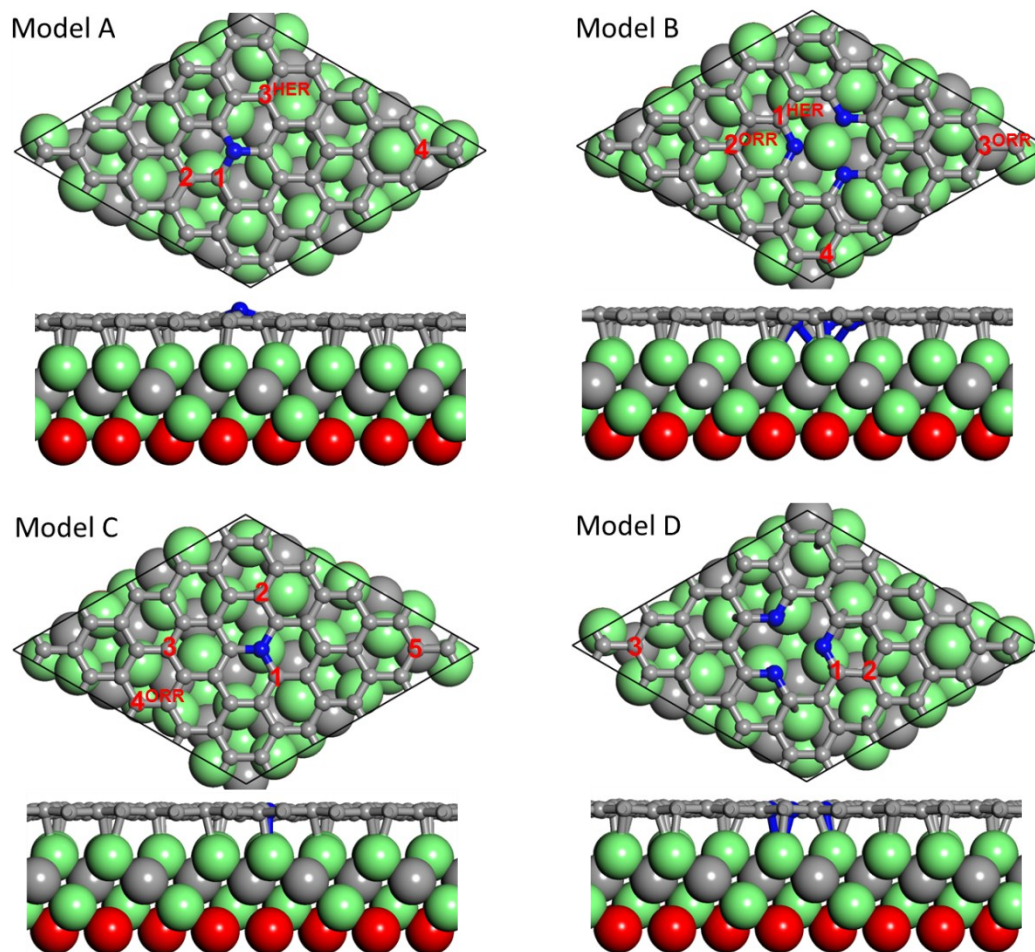


Fig. S2 Same as Fig. S1 for N-doped graphene on V_2C MXene monolayer. The binding energies of reaction intermediates and activities for ORR and HER are listed in Table S4. The V atoms are shown in green.

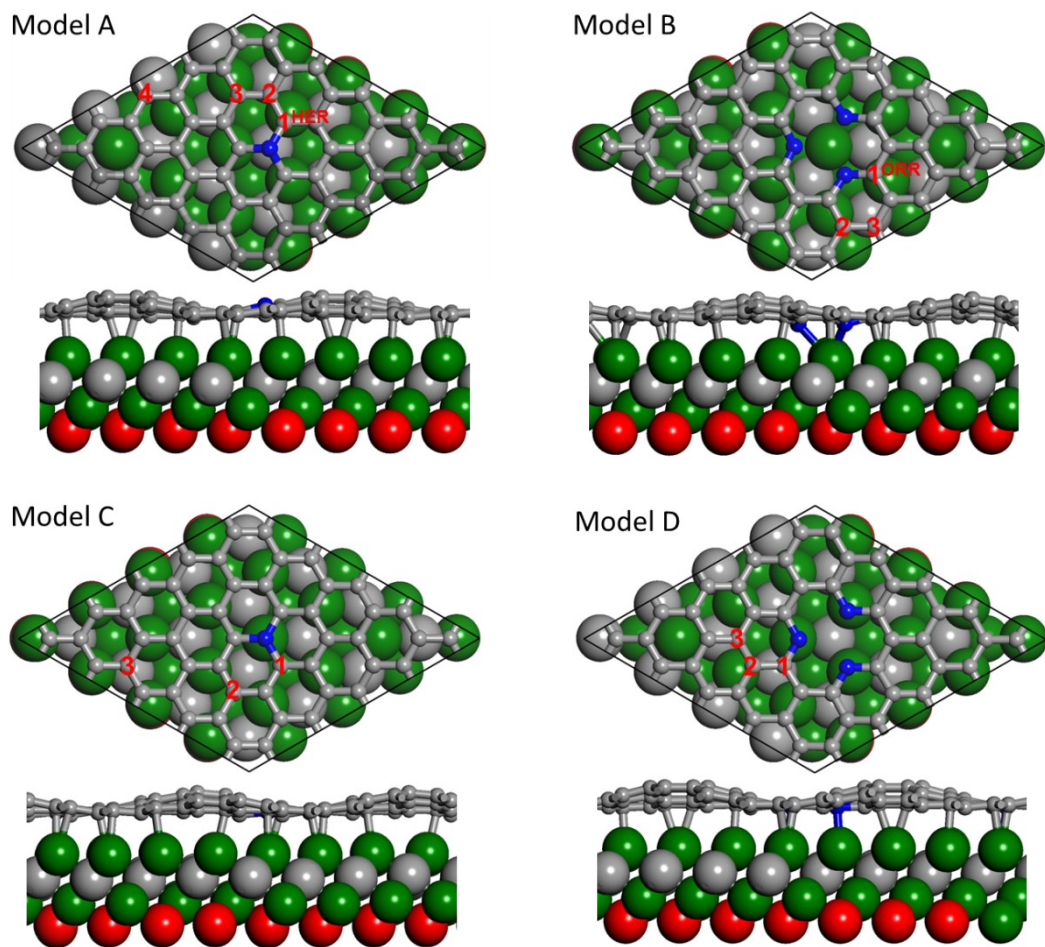


Fig. S3 Same as Fig. S1 for N-doped graphene on Nb₂C MXene monolayer. The binding energies of reaction intermediates and activities for ORR and HER are listed in Table S5. The Nb atoms are shown in dark green.

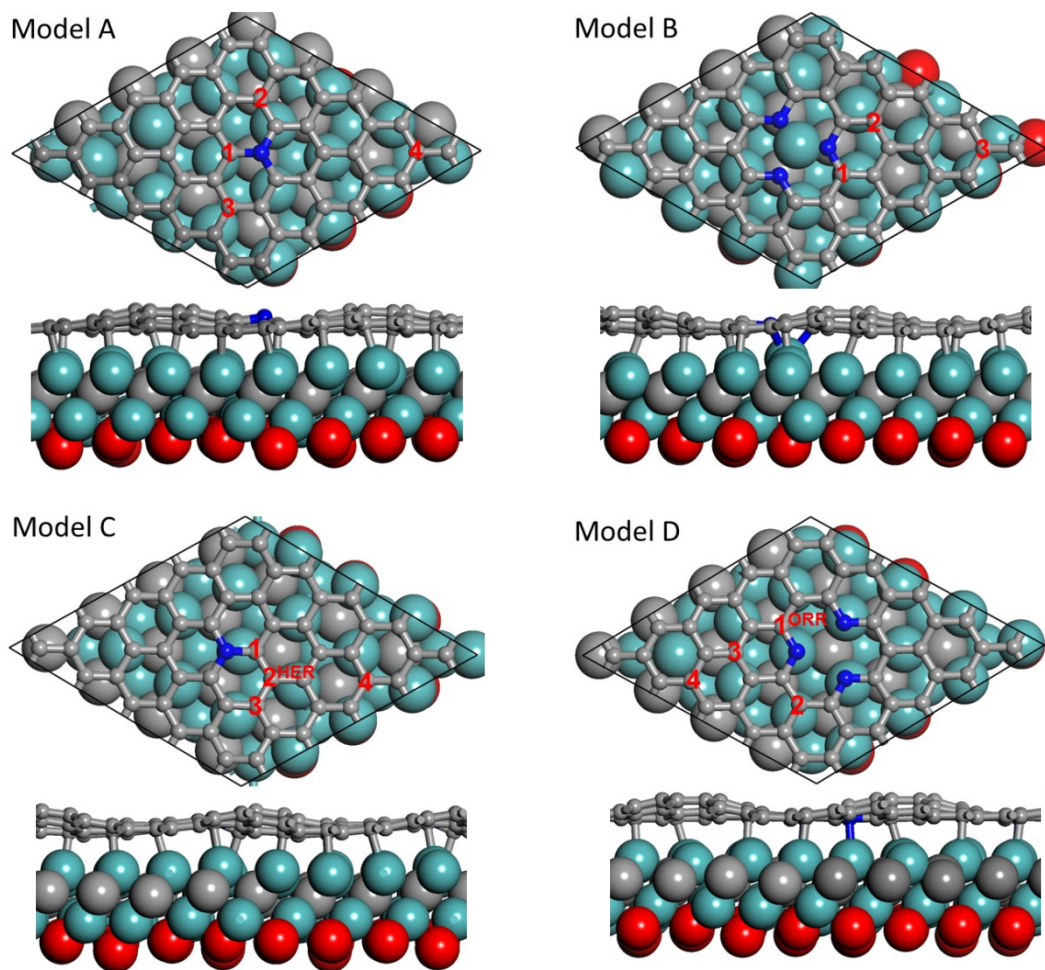


Fig. S4 Same as Fig. S1 for N-doped graphene on Mo₂C MXene monolayer. The binding energies of reaction intermediates and activities for ORR and HER are listed in Table S6. The Mo atoms are shown in turquoise.

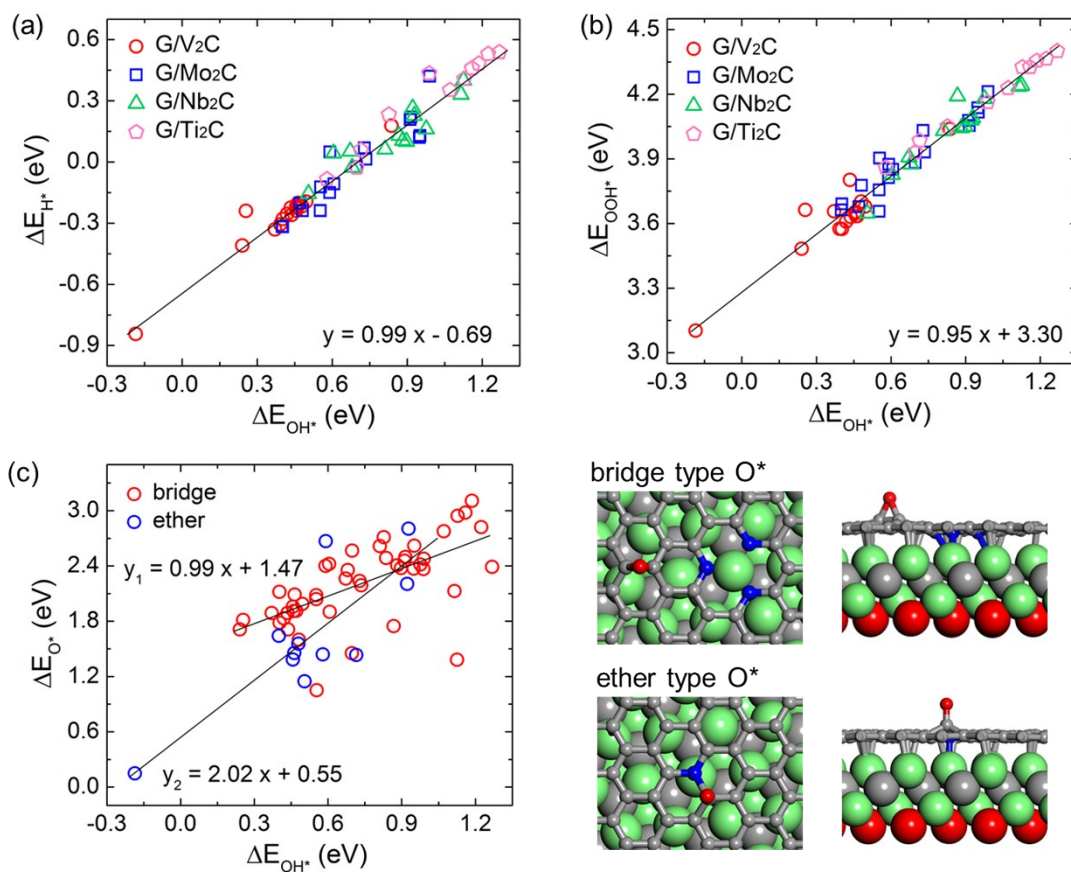


Fig. S5 Linear relations of binding energies of (a) H^* vs. OH^* , (b) OOH^* vs. OH^* , and (c) O^* vs. OH^* species for the graphene/MXene heterostructures. The black lines are linear fitting of the data points. In panel (c), the binding energies of O^* species in the bridge and ether type configurations follow different linear relations. Their atomic structures (top and side views) are shown on the right.

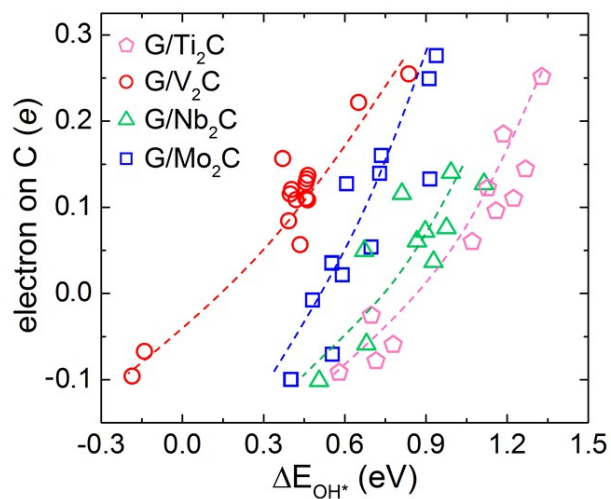


Fig. S6 Number of electrons gained by each surface C atom as a function of OH* binding energy for various graphene/MXene heterostructures. The colored dashed lines are guide for eyes.

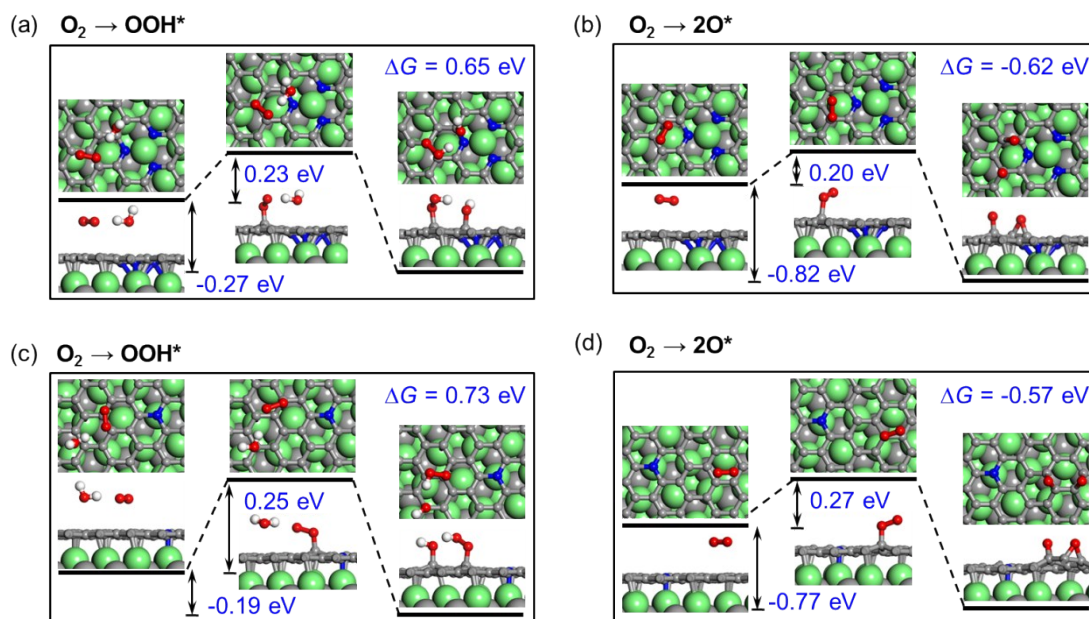


Fig. S7 Dual reaction pathways for ORR on the G/V₂C heterostructures with the N dopants in (a, b) pyridinic form and (c, d) graphitic form, respectively. The insets show the atomic structures of the initial (left), transition (middle) and final states (right), respectively. The blue numbers (from left to right) indicate the total energy change during the reaction, kinetic barrier and Gibbs free energy of formation, respectively. The C, N, O and V atoms are shown in grey, blue, red and green colors, respectively. In the transition states, the adsorbed oxygen dimer has O–O bond length of 1.28 and 1.30 Å, and C–O distance of 1.70 and 1.81 Å (C is underneath O atom) for the O₂ → OOH* and O₂ → 2O* reaction pathways, respectively. For both pathways, the oxygen dimer is in the spin singlet state. In contrast, on the standalone N-doped graphene, the transition state of O₂ → 2O* reaction involves two O atoms adsorbed on the top site of C atoms with O–O distance of 1.85 Å and energy barrier of 1.20 eV.¹⁰

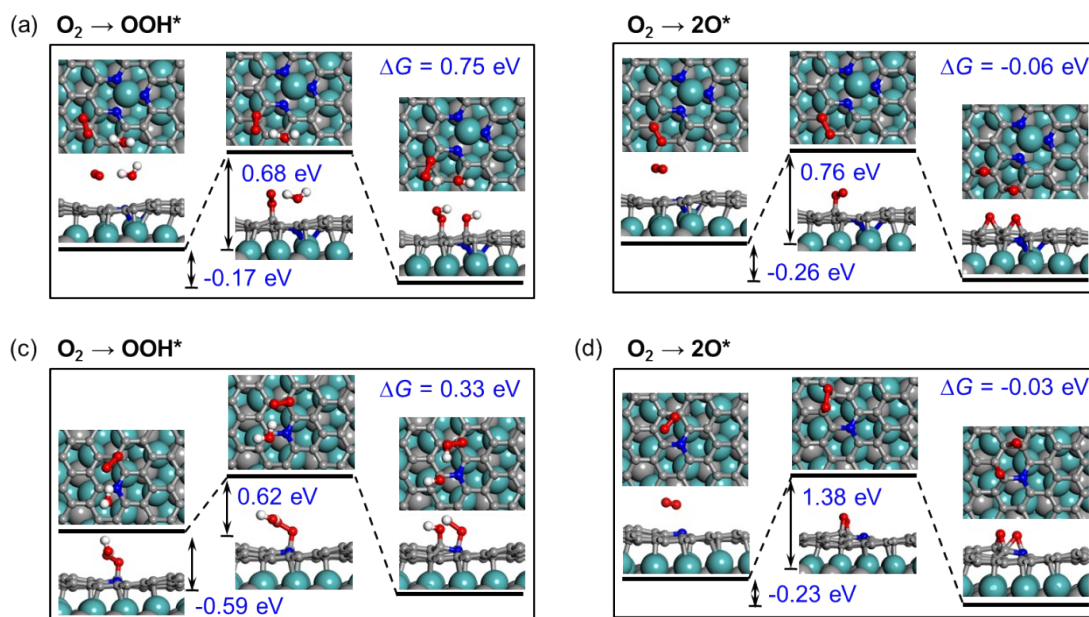


Fig. S8 Same as Fig. S7 for the G/Mo₂C heterostructures. The Mo atoms are shown in turquoise. In the transition states, the adsorbed oxygen dimer has O–O bond length of 1.37 and 1.36 Å, and C–O distance of 1.87 and 1.60 Å (C is underneath O atom) for the $\text{O}_2 \rightarrow \text{OOH}^*$ and $\text{O}_2 \rightarrow 2\text{O}^*$ reaction pathways, respectively. For both pathways, the oxygen dimer is in the spin singlet state.

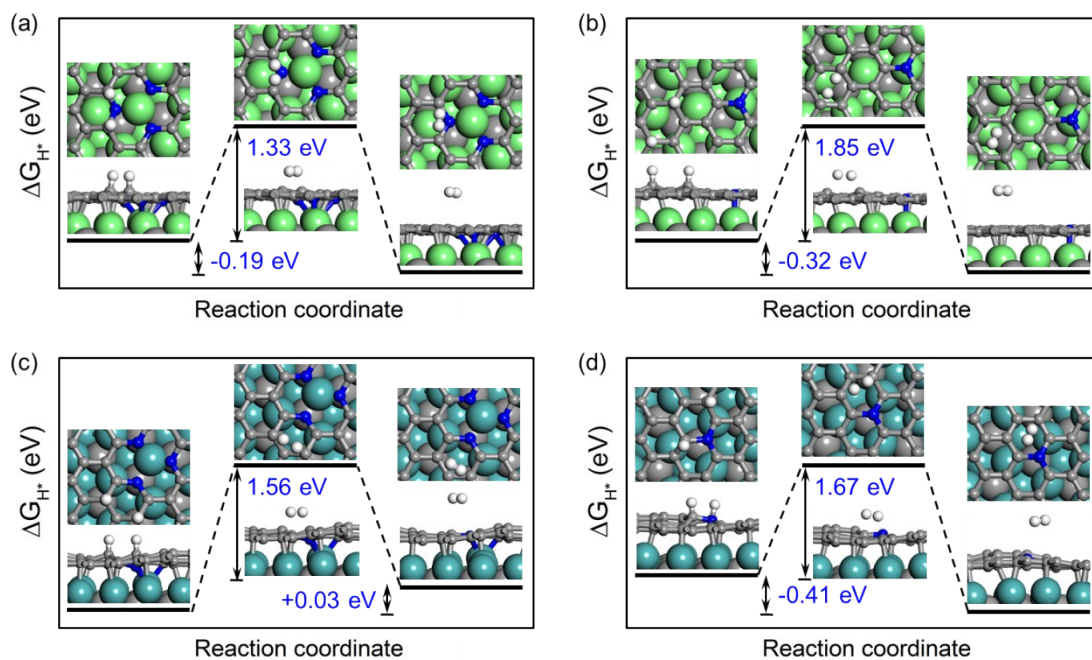


Fig. S9 Changes of ΔG_{H^*} during HER on (a, b) G/V₂C and (c, d) G/Mo₂C heterostructures. The insets show (from left to right) the atomic structures of the initial, transition and final states, respectively. The H, C, N, V and Mo atoms are shown in white, grey, blue, green and turquoise colors, respectively.

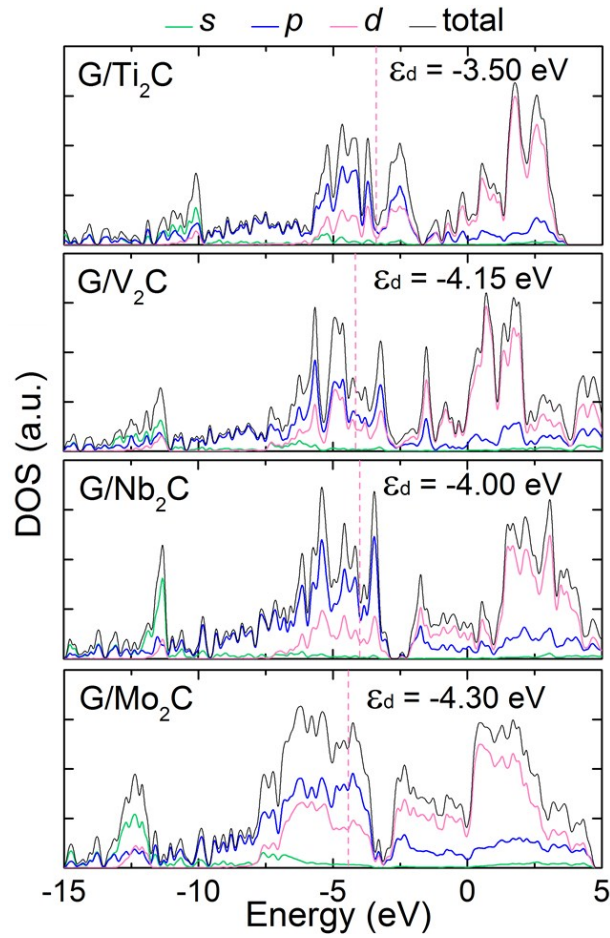


Fig. S10 Density of states (DOS) of various graphene/MXene heterostructures. The colored lines show the projected DOS from different atomic orbitals. The pink dashed lines and the numbers next to them indicate the *d* band center relative to the Fermi level.

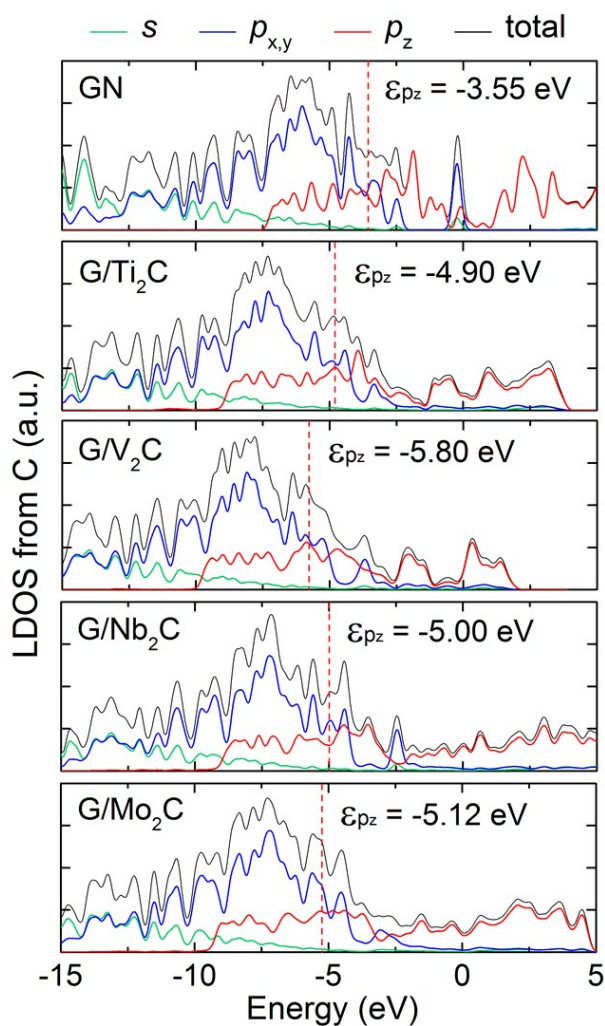


Fig. S11 Local density of states (LDOS) of surface C atoms from freestanding N-doped graphene (GN) and the one supported by various MXene monolayers. The N atoms are in the pyridinic form. The colored lines show the projected DOS from different atomic orbitals. The red dashed lines and the numbers next to them indicate the p_z band center relative to the Fermi level.

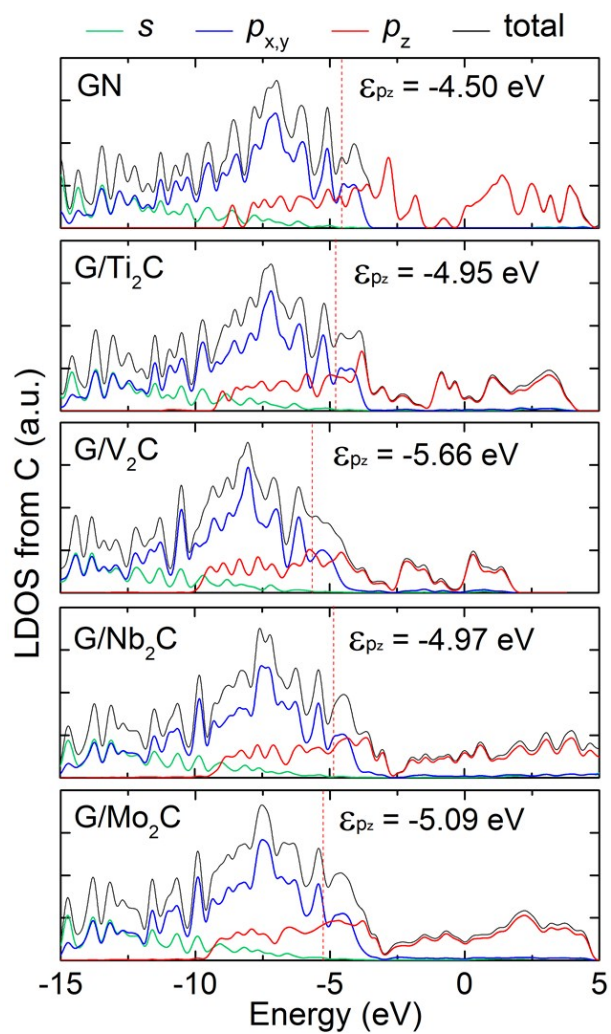


Fig. S12 Same as Fig. S11 with the N dopants in the graphitic form.

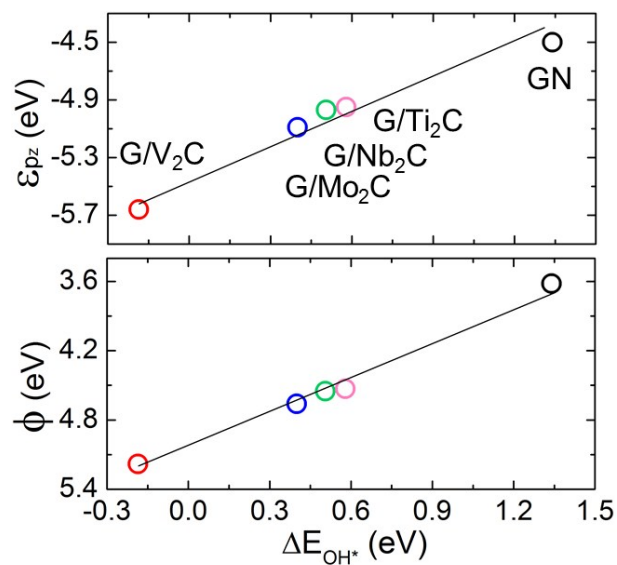


Fig. S13 The C p_z band center (top panel) and work function (bottom panel) as a function of lowest binding energies of OH* species for various graphene/MXene heterostructures and for freestanding N-doped graphene (GN). The N atoms are in the graphitic form.

References

- 1 M. del Cueto, P. Ocón and J. M. L. Poyato, *J. Phys. Chem. C*, 2015, **119**, 2004-2009.
- 2 M. W. Chase, JANAF thermochemical table[J]. *J. Phys. Chem. Ref. Data* 1985, **14**, Supplement No. 1.
- 3 J. Rossmeisl, Z. W. Qu, H. Zhu, G. J. Kroes and J. K. Nørskov, *J. Electroanal. Chem.*, 2007, **607**, 83-89.
- 4 Y.-F. Li and A. Selloni, *ACS Catal.*, 2014, **4**, 1148-1153.
- 5 S. Zhou, N. Liu, Z. Wang and J. Zhao, *ACS Appl. Mater. Interfaces*, 2017, **9**, 22578-22587.
- 6 J. K. Nørskov, T. Bligaard, A. Logadottir, J. R. Kitchin, J. G. Chen, S. Pandalov and U. Stimming, *J. Electrochem. Soc.*, 2005, **152**, J23-J26.
- 7 R. Hoffmann, *J. Chem. Phys.*, 1963, **39**, 1397-1412.
- 8 G. Gao, A. P. O'Mullane and A. Du, *ACS Catal.*, 2017, **7**, 494-500.
- 9 Z. Seh, K. D. Fredrickson, B. Anasori, J. Kibsgaard, A. L. Strickler, M. R. Lukatskaya, Y. Gogotsi, T. F. Jaramillo and A. Vojvodic, *ACS Energy Lett.*, 2016, **1**, 589-594.
- 10 H. J. Yan, B. Xu, S. Q. Shi and C. Y. Ouyang, *J. Appl. Phys.*, 2012, **112**, 104316.